Constraints on the Cosmic Expansion Rate at Redshift 2.3 from the Lyman-α Forest

Andrei Cuceu,[1,2,3,4,*] Andreu Font-Ribera,[5,4] Seshadri Nadathur,[6] Benjamin Joachimi,[4] and Paul Martini[2,1]
[1]Center for Cosmology and Astro-Particle Physics, The Ohio State University, Columbus, Ohio 43210, USA
[2]Department of Astronomy, The Ohio State University, Columbus, Ohio 43210, USA
[3]Department of Physics, The Ohio State University, Columbus, Ohio 43210, USA
[4]Department of Physics and Astronomy, University College London, Gower Street, London WC1E 6BT, United Kingdom
[5]Institut de Física d'Altes Energies, The Barcelona Institute of Science and Technology, Campus UAB, 08193 Bellaterra (Barcelona), Spain
[6]Institute of Cosmology and Gravitation, University of Portsmouth, Burnaby Road, Portsmouth, PO1 3FX, United Kingdom

(Received 28 September 2022; revised 23 December 2022; accepted 9 February 2023; published 12 May 2023)

We determine the product of the expansion rate and angular-diameter distance at redshift $z = 2.3$ from the anisotropy of Lyman-α (Lyα) forest correlations measured by the Sloan Digital Sky Survey (SDSS). Our result is the most precise from large-scale structure at $z > 1$. Using the flat Λ cold dark matter model we determine the matter density to be $\Omega_m = 0.36^{+0.03}_{-0.04}$ from Lyα alone. This is a factor of 2 tighter than baryon acoustic oscillation results from the same data due to our use of a wide range of scales ($25 < r < 180\ h^{-1}$ Mpc). Using a nucleosynthesis prior, we measure the Hubble constant to be $H_0 = 63.2 \pm 2.5$ km/s/Mpc. In combination with other SDSS tracers, we find $H_0 = 67.2 \pm 0.9$ km/s/Mpc and measure the dark energy equation-of-state parameter to be $w = -0.90 \pm 0.12$. Our Letter opens a new avenue for constraining cosmology at high redshift.

DOI: 10.1103/PhysRevLett.130.191003

Introduction.—Over the last few decades the Λ cold dark matter model (ΛCDM) has become the standard model of cosmology. However, increased precision in cosmological measurements gave rise to tensions between different probes, highlighting potential shortcomings in the standard model. The most discussed of these is the $\sim 5\sigma$ discrepancy between the value of the Hubble constant H_0, inferred from cosmic microwave background (CMB) measurements by the Planck satellite [1] (which assume ΛCDM), and local measurements using the cosmic distance ladder [2]. Furthermore, the most important component of ΛCDM at the present time, dark energy, is still not theoretically understood. On the observational side, the main way to address these challenges is to measure the expansion rate with greater precision through different probes, and at different stages of the evolution of the Universe.

Probes of large-scale structure (LSS) currently provide some of the tightest constraints on the expansion rate after recombination (e.g., Refs. [3–12]). While many of these measurements focus on the baryon acoustic oscillation (BAO) feature as a standard ruler [13,14], the clustering of LSS tracers contains important information beyond BAO. At low redshift, $z < 1.5$, analyses of the two-point statistics of galaxies improve on BAO constraints by using information from a wider range of scales, at the expense of including more model assumptions (e.g., Refs. [4–7,15,16]). Usually these analyses take advantage of the Alcock-Paczyński (AP; [17]) effect, the power of which has been demonstrated by Refs. [11,18], using voids. This effect adds an anisotropy on all scales in the LSS distribution if the fiducial cosmology used to compute comoving distances from angles and redshifts is different from the truth. Therefore, a measurement of this apparent anisotropy can help determine the true cosmology. This effect is usually also measured in BAO analyses, but only using a small fraction of the available information (around the BAO peak). At high redshifts, $z > 1.5$, where the Lyman-α (Lyα) forest is used as a continuous tracer of the LSS, the best constraints currently come from the BAO scale alone [8,19].

We measure the AP effect for the first time using a broad range of scales in the three-dimensional Lyα forest correlation functions. We use data from the Sloan Digital Sky Survey (SDSS) data release 16 (DR16; [20]), which includes measurements from the Baryon Oscillation Spectroscopic Survey (BOSS; [21]), and its successor, extended BOSS (eBOSS; [22]). Furthermore, we examine the cosmological constraints derived from this measurement alone and in combination with other SDSS tracers at lower redshift.

Methods and data.—We use the Lyα forest three-dimensional correlation functions computed by the eBOSS collaboration using SDSS Data Release 16 [19], and focus on extracting the AP information from the anisotropy in these correlations. Our tracers include Lyα flux in the Lyα region (between the Lyα and Lyβ peaks), denoted Lyα(Lyα); Lyα flux in the Lyman-β (Lyβ) region (blue ward of the Lyβ peak), denoted Lyα(Lyβ); and the quasar distribution (QSO; [23]). In total we use four correlation

functions, which for modeling purposes are categorized into two Lyα auto-correlations, Lyα(Lyα) $\times$ Lyα(Lyα) and Lyα(Lyα) $\times$ Lyα(Lyβ), and two Lyα-QSO cross-correlations, Lyα(Lyα) $\times$ QSO and Lyα(Lyβ) $\times$ QSO. We perform a joint fit of the full shapes of these four correlations in order to extract the AP effect. We use the term *full-shape* (FS) to refer to the extraction of cosmological information from a broad range of scales in the correlation function (that includes BAO), rather than just the BAO peak alone.

Our model of the Lyα correlation functions broadly follows the framework used by BOSS and eBOSS in past BAO analyses. We use a template approach based on a fiducial cosmology, starting from an isotropic linear matter power spectrum, computed using CAMB [24]. This template is decomposed into a peak and a smooth component following [25]. The Lyα modeling is applied independently to the two components, and they are combined only at the end to build the full correlation model. The key ingredients of this model are the linear Lyα and QSO biases and redshift space distortions (RSD), along with the AP effect (see Refs. [19,25,26]).

We compute the correlation models and the Gaussian likelihood with the Vega package [27], using the same models and parameters for the contaminants as in eBOSS [19,26]. See the Supplemental Material [28] for more details on the data, model, and likelihood, which includes Refs. [29–46]. We sample posterior distributions using the Nested Sampler PolyChord [47,48].

In BAO analyses, the coordinates of the peak component are allowed to vary anisotropically, in order to fit both the BAO scale and the AP effect from the peak position. Here we also vary the coordinates of the smooth component in order to extract AP from the full correlation. As the AP effect introduces an anisotropy in the correlation function, we follow Ref. [39] and introduce the parameters

$$\phi(z) \equiv \frac{q_\perp(z)}{q_{||}(z)} \quad \text{and} \quad \alpha(z) \equiv \sqrt{q_\perp(z) q_{||}(z)}, \qquad (1)$$

where $q_{||}$ and $q_\perp$ rescale the comoving coordinates, $r_{||}$ and $r_\perp$, along and across the line of sight, respectively. ϕ measures the anisotropy, and therefore the AP effect, while α measures the isotropic scale [49]. As we have two components, we have the option of using two sets of these parameters, one for the peak component (ϕ_p, α_p) and one for the smooth component (ϕ_s, α_s). This is appropriate for α, where the cosmological information comes from the BAO scale (α_p), while α_s is treated as a nuisance. On the other hand, both ϕ_p and ϕ_s measure the same effect (AP), and therefore our baseline analysis uses one coherent parameter for both components, denoted ϕ_f. However, the two ϕ parameters are still useful for distinguishing the BAO measurement from the broadband information, as they are affected by different contaminants [39].

The main contaminants affecting Lyα forest correlations are high column density absorbers, metal absorbers, and the distortion due to quasar continuum fitting. We model these contaminants following the approach used by BOSS and eBOSS BAO analyses [19,30,31]. Following Ref. [19], we model deviations from linear theory in the Lyα autocorrelation using the multiplicative correction proposed by Ref. [36]. For the Lyα-QSO cross-correlation, we also follow Ref. [19], and use a Lorentzian damping term [38] to model both the redshift errors and the Finger-of-God effect in the cross-correlation.

In order to validate our method, we performed a detailed analysis on synthetic data using 100 eBOSS mock realizations. The results on synthetic data and a detailed description of our methodology are presented in Ref. [26] (also see the Supplemental Material [28]). The main Lyα forest contaminants are simulated in these synthetic data, and we found that our method results in unbiased AP measurements when fitting scales between 25 h^{-1} Mpc and 180 h^{-1} Mpc [26]. Based on these results, we use a minimum scale $r_{\rm min} = 25\ h^{-1}$ Mpc. This restricts our analysis to large scales, reducing the impact of nonlinearities.

We discussed additional sources of contamination, not currently included in state-of-the-art Lyα forest mocks, in Ref. [26]. The most important of these are deviations from linear theory, and realistic redshift errors [26]. Lyα forest nonlinearities have been recently studied by Ref. [37] using hydrodynamical simulations, and in the case of the Lyα autocorrelation were found to be well modeled by the empirical relation introduced by Ref. [36]. On the other hand, for the Lyα-QSO cross-correlation the QSO redshift errors generally dominate on small scales. We discuss this in more detail in the Supplemental Material [28].

We also tested the sensitivity of our result to different analysis choices, focusing on robustness tests for ϕ_s, as tests for α_p and ϕ_p (using a different parametrization) were done by Ref. [19]. We blinded our analysis by adding a random value to our ϕ_s measurement, such that we did not know the true result until we chose the exact configuration of our baseline model. We tested a variety of modeling options, presented in the Supplemental Material [28], and found that our result is robust to these changes. The only noteworthy deviation happens when changing the model for QSO redshift errors. While our baseline analysis uses a Lorentzian damping term, we found a $\sim 0.5\sigma$ shift in our ϕ_s measurement when using a Gaussian damping term instead. As the distribution of quasar redshift errors has long tails [23], we followed Ref. [19] and chose the Lorentzian damping in our baseline analysis.

The joint fit of the four Lyα correlation functions using the baseline model produces a good fit, with $\chi^2_{\rm min} = 9391.85$ for 9363 degrees of freedom (PTE = 0.41). The fit quality is consistent between mocks and data, with 38% of the mock realizations giving a lower χ^2 value. Figure 1 shows the data and best-fit model for our main correlation,

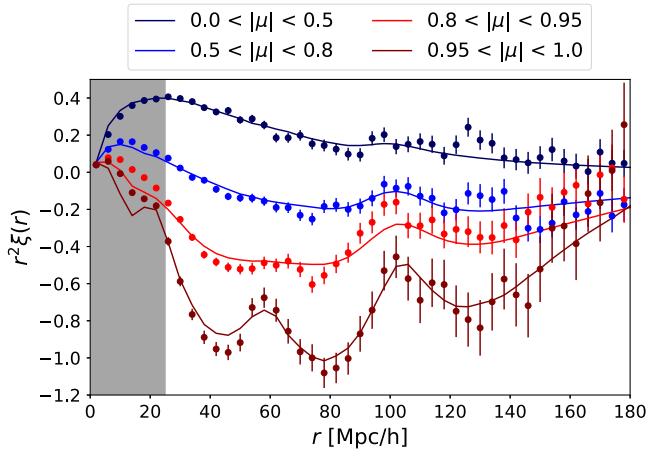

FIG. 1. The eBOSS Lyα forest autocorrelation function ξ (points with error bars) and the best-fit model, as a function of comoving separation r. For illustration, the correlation function is compressed into four bins in the cosine of the line-of-sight angle μ. The gray area shows the small scales which we exclude from the fit. The Alcock-Paczyński effect is extracted from the anisotropy in the correlation (its dependence on μ).

Lyα(Lyα) $\times$ Lyα(Lyα). As our data and model are 2D functions of $r_{\parallel}$ and $r_{\perp}$, we compress them into four $\mu = r_{\parallel}/r$ bins, and show them as a function of isotropic separation $r = \sqrt{r_{\parallel}^2 + r_{\perp}^2}$, for visualization purposes.

To better understand the AP effect and where this information comes from, we also compress the correlation function into shells in r, and plot them as a function of μ. One such example is shown in Fig. 2, where we choose the smallest separation shell ($25 < r < 45\ h^{-1}$ Mpc) of the Lyα(Lyα) $\times$ Lyα(Lyα) correlation. This figure illustrates

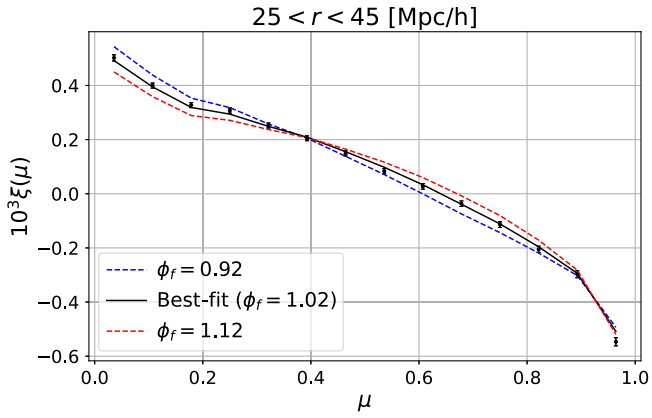

FIG. 2. Lyα forest autocorrelation function (points with error bars) in a shell at separation r, shown as a function of the cosine of the line-of-sight angle, μ. We compare the best-fit model (black) with two other models where the ϕ_f parameter, which measures the AP effect relative to the fiducial cosmology, takes different values (red and blue). This illustrates how the AP effect is constrained.

how the model changes for different values of ϕ_f, showing that the AP information comes in large part from intermediate and small values of μ, rather than the line-of-sight region ($\mu = 1$) where most Lyα forest contaminants have an impact. Shells for larger separations and also showing the impact of RSD are included in the Supplemental Material [28].

Results.—After unblinding, we can compare ϕ results when fitting two separate parameters for the peak and smooth components (ϕ_p and ϕ_s), and when we only fit one shared parameter (ϕ_f). The main results of this Letter are the AP measurements from the broadband (ϕ_s), and the full-shape measurement (ϕ_f). The three results are

$$\text{BAO AP: } \phi_p = 0.933 \pm 0.041, \tag{2}$$

$$\text{Broadband AP: } \phi_s = 1.037 \pm 0.020, \tag{3}$$

$$\text{Full shape AP: } \phi_f = 1.021 \pm 0.019. \tag{4}$$

As our fiducial cosmology is based on Planck CMB results, $\phi = 1$ represents the best-fit Planck cosmology. Lyα BAO measurements from BOSS and eBOSS have resulted in ϕ values smaller than 1 [19]. Our BAO AP measurement is 1.7σ lower than the Planck best-fit value, consistent with the result obtained by Ref. [19] using the same dataset and matching scale cuts. On the other hand, our broadband AP result gives a value 1.9σ higher than Planck [50].

While individually both ϕ_p and ϕ_s are consistent with Planck, they are in 2.3σ tension with each other. Our result for ϕ_s is robust to changes in the modeling (see Supplemental Material [28]). The biggest shift, coming from changing the model for QSO redshift errors, only reduces the tension with BAO from 2.3 to 2.0σ. As our baseline model for the errors is more realistic, we kept the preunblinding model choices when inferring cosmology.

Our final measurement is given by the ϕ_f constraint, which combines BAO and broadband information. Fitting the full shape of Lyα correlation functions results in a factor of 2 improvement in constraining power over the BAO-only constraint measured by Ref. [19].

In addition to ϕ_f, we also infer cosmology from the isotropic BAO scale, which we measure to be $\alpha_p = 1.017 \pm 0.014$. This differs slightly from the value reported by Ref. [19], $\alpha_p = 1.000 \pm 0.014$, due to the use of different scale cuts and the correlation between ϕ_f and α_p (Pearson correlation coefficient of 0.21). The two-dimensional posterior of these parameters is well approximated by a multivariate Gaussian, and therefore, we use this Gaussian result in the analysis below.

Inferring cosmology.—Our ϕ_f and α_p measurements represent ratios between distances measured using the assumed fiducial cosmological model and the true cosmology. Following Ref. [39], these are given by

$$\text{AP: } \phi = \frac{D_M(z)H(z)}{[D_M(z)H(z)]_{\text{fid}}}, \tag{5}$$

$$\text{BAO: } \alpha = \sqrt{\frac{D_M(z)D_H(z)/r_d^2}{[D_M(z)D_H(z)/r_d^2]_{\text{fid}}}}, \tag{6}$$

where D_M is the transverse comoving distance, $H(z)$ is the Hubble parameter, r_d is the size of the acoustic scale, and $D_H = c/H$, with the speed of light, c. The effective redshift of our measurement is $z = 2.33$. We use the Gaussian likelihood in ϕ and α above together with Eqs. (5) and (6) to derive constraints on cosmological parameters through Monte Carlo Markov Chain sampling of model posteriors with Cobaya [45,46].

For completeness, we also report our measurement in terms of the usual ratios: $D_H(z = 2.33)/r_d = 8.65 \pm 0.13$ and $D_M(z = 2.33)/r_d = 40.26 \pm 0.71$. Using the Planck measured value of $r_d = 147.05 \pm 0.30$ Mpc [1], we determine the expansion rate at redshift 2.33 to be $H(z = 2.33) = 235.9 \pm 3.5$ km s^{-1} Mpc^{-1}.

We also compare and combine our measurement with results from other datasets, including the full-shape results from lower-redshift SDSS tracers and CMB anisotropy measurements by Planck. We sample the posteriors for combinations of these likelihoods using parameter choices and priors following Ref. [8]. For SDSS, we use the "BAO-plus" likelihoods which include BAO and full-shape information from BOSS and eBOSS, including the latest data from DR16 [8]. We also use the public Planck chains [51] where appropriate for comparison purposes.

Flat ΛCDM.—In flat ΛCDM, measurements of the isotropic BAO scale (α_p) constrain a combination of $\Omega_{\rm m}$ and $H_0 r_d$. This degeneracy can be broken by the AP measurement of ϕ, which directly translates to a constraint on $\Omega_{\rm m}$. Our Lyα full-shape result, ϕ_f, corresponds to $\Omega_{\rm m} = 0.36^{+0.03}_{-0.04}$. This is a factor of 2 higher precision than obtained from previous BAO-only results [19] and produces our substantially improved cosmological constraints.

In order to measure the Hubble constant, H_0, from the degenerate combination $H_0 r_d$, we require the value of r_d. This depends on the total matter density, the baryon density, and the neutrino density [52]. We fix the neutrino density by assuming degenerate mass eigenstates with total mass $\Sigma m_\nu = 0.06$ eV$/c^2$, and assume a prior on the baryon density, $\Omega_b h^2 = 0.02233 \pm 0.00036$, based on measurements of the primordial deuterium to hydrogen ratio and big bang nucleosynthesis (BBN; [53,54]). With these priors, we measure H_0 from our results of α_p and ϕ_f, independently of information from Planck CMB anisotropies.

In Fig. 3 we show posterior distributions of $\Omega_{\rm m}$ and H_0. The two main cosmological constraints in this Letter are

$$\text{Ly}\alpha\text{ FS: } H_0 = 63.2 \pm 2.5 \text{ km s}^{-1}\text{ Mpc}^{-1}, \tag{7}$$

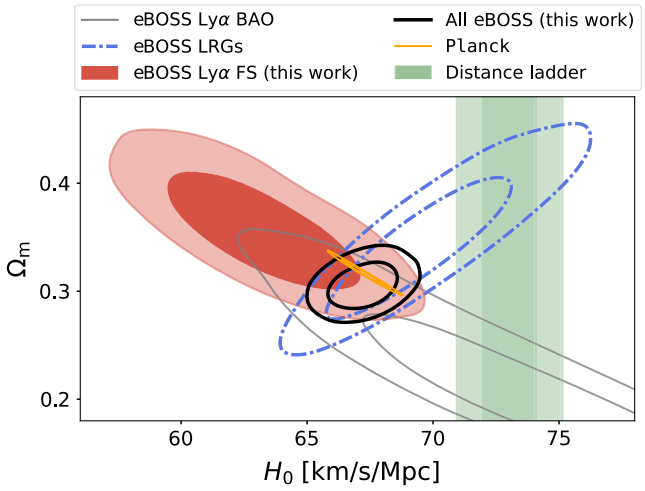

FIG. 3. Marginalized 68 and 95% contours on $\Omega_{\rm m}$ and H_0, assuming ΛCDM. The eBOSS results assume a BBN prior on the baryon density. These results are independent of CMB anisotropy measurements, but are consistent with Planck and in tension with the distance ladder results of Ref. [2].

$$\text{All eBOSS: } H_0 = 67.23 \pm 0.91 \text{ km s}^{-1}\text{ Mpc}^{-1}. \tag{8}$$

Lyα forest constraints alone result in a tight measurement of H_0, comparable to that from the most powerful single probe in SDSS, luminous red galaxies (LRG). Interestingly, we obtain a low measurement of the Hubble constant, which is in 3.6σ tension with the direct result from the distance ladder [2], but still compatible with Planck at the 1.6σ level. When combining our measurement with results from other eBOSS tracers, we obtain a tight posterior that is

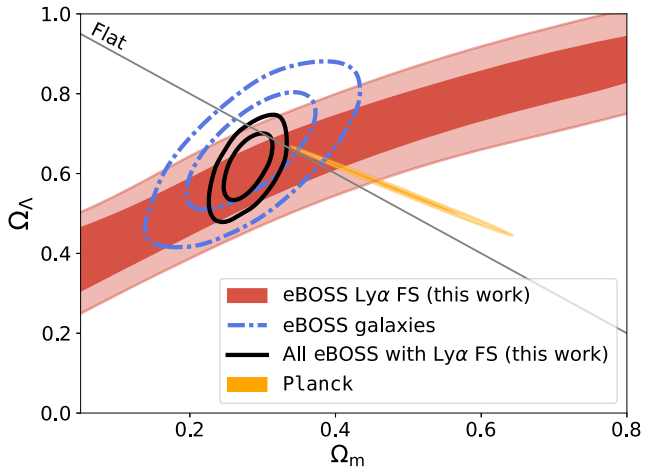

FIG. 4. Marginalized constraints on the dark energy density parameter Ω_Λ, versus $\Omega_{\rm m}$ from Lyα, eBOSS galaxies, and Planck, under the assumption that dark energy is described by the cosmological constant. The addition of the Lyα measurement improves on the eBOSS galaxies' constraint by a factor of 2 and results in a $> 12\sigma$ detection of the late-time accelerated expansion of the Universe.

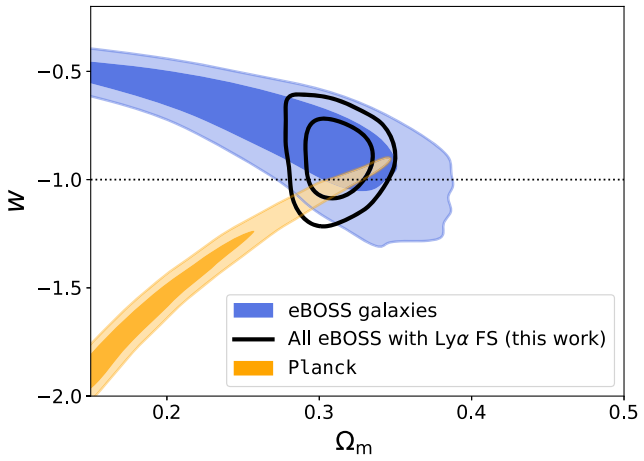

FIG. 5. Constraints on the dark energy equation of state parameter w from eBOSS galaxies alone and combined with our Lyα full-shape measurement. Adding Lyα results in a $\sim$12% measurement of w from SDSS alone. This is independent of Planck constraints.

compatible with Planck and in 4.2σ tension with the distance ladder. Finally, the improvement in constraining power when performing a full-shape analysis of the Lyα correlations can be seen from the difference between the gray and the red posteriors in Fig. 3.

Dark energy and curvature.—We next relax the assumption that the Universe is flat and allow the curvature parameter Ω_k to vary. We still assume dark energy is described by the cosmological constant, which means its equation of state parameter is $w = -1$. We show our measurements of Ω_Λ versus Ω_m in Fig. 4, where we do not include any external prior, as we directly sample the combination $H_0 r_d$. The Lyα forest constrains a degenerate posterior between Ω_m and Ω_Λ that nevertheless excludes $\Omega_\Lambda = 0$ at $> 4\sigma$ level.

When combined with the other eBOSS tracers, we measure $\Omega_\Lambda = 0.62^{+0.06}_{-0.05}$, and $\Omega_k = 0.10 \pm 0.07$. Our results are compatible with the Universe today being flat and dominated by dark energy. We find direct geometrical evidence of late-time acceleration due to dark energy at the $>12\sigma$ level.

Finally, we consider models where w is allowed to vary, and Ω_k is fixed to zero. We present our results in Fig. 5, where we focus on SDSS measurements. The eBOSS galaxies' full-shape measurements result in a partially degenerate posterior between w and Ω_m. Adding our Lyα full-shape measurement breaks this degeneracy, and we measure $w = -0.90 \pm 0.12$, consistent with the late-time acceleration being caused by a cosmological constant dark energy. We emphasize that this result only depends on SDSS data, which sets this experiment apart in its ability to constrain dark energy without needing other datasets.

Conclusions.—We present the first cosmological measurement from a broad range of spatial scales in the Lyα forest three-dimensional correlations, through the Alcock-Paczyński effect. Using eBOSS DR16 data, we obtain the tightest cosmological constraints to date from large-scale structure at $z > 1$, shown through our constraints on H_0 and the late-time accelerated expansion.

Key areas of future improvement include better modeling of quasar redshift errors and a better understanding of the impact of nonlinearities. Furthermore, Lyα forest correlation functions could also be used to measure the growth of cosmic structure as proposed by Refs. [39,55]. Our measurement opens a new avenue for constraining cosmology at high redshifts ($2 < z < 4$) with future surveys such as the ongoing Dark Energy Spectroscopic Instrument [44].

We thank James Rich, David H. Weinberg, and Naim Göksel Karaçaylı for useful discussion and comments during the preparation of this manuscript. A. C. and P. M. acknowledge support from the United States Department of Energy, Office of High Energy Physics under Award No. DE-SC-0011726. A. F. R. acknowledges support through the program Ramon y Cajal (RYC-2018-025210) of the Spanish Ministry of Science and Innovation and from the European Union's Horizon Europe research and innovation program (COSMO-LYA, Grant Agreement No. 101044612). IFAE is partially funded by the CERCA program of the Generalitat de Catalunya. S. N. acknowledges support from an STFC Ernest Rutherford Fellowship, Grant Reference No. ST/T005009/2. B. J. acknowledges support by STFC Consolidated Grant No. ST/V000780/1. We acknowledge the use of the GETDIST [56] and NUMPY [57] packages.

*cuceu.1@osu.edu

[1] N. Aghanim, Y. Akrami, M. Ashdown, J. Aumont, C. Baccigalupi, M. Ballardini, A. J. Banday, R. B. Barreiro, N. Bartolo, S. Basak, R. Battye, K. Benabed, J. P. Bernard, M. Bersanelli *et al.* (Planck Collaboration), Astron. Astrophys. **641**, A6 (2020).

[2] A. G. Riess, W. Yuan, L. M. Macri, D. Scolnic, D. Brout, S. Casertano, D. O. Jones, Y. Murakami, L. Breuval, T. G. Brink, A. V. Filippenko, S. Hoffmann, S. W. Jha, W. D. Kenworthy, G. Anand *et al.*, Astrophys. J. Lett. **934**, L7 (2022).

[3] S. Alam, M. Ata, S. Bailey, F. Beutler, D. Bizyaev, J. A. Blazek, A. S. Bolton, J. R. Brownstein, A. Burden, C.-H. Chuang, J. Comparat, A. J. Cuesta, K. S. Dawson, D. J. Eisenstein, S. Escoffier *et al.*, Mon. Not. R. Astron. Soc. **470**, 2617 (2017).

[4] H. Gil-Marín, J. E. Bautista, R. Paviot, M. Vargas-Magaña, S. de la Torre, S. Fromenteau, S. Alam, S. Ávila, E. Burtin, C.-H. Chuang, K. S. Dawson, J. Hou, A. de Mattia, F. G. Mohammad, E.-M. Müller *et al.*, Mon. Not. R. Astron. Soc. **498**, 2492 (2020).

[5] J. E. Bautista, R. Paviot, M. Vargas Magaña, S. de la Torre, S. Fromenteau, H. Gil-Marín, A. J. Ross, E. Burtin, K. S. Dawson, J. Hou, J.-P. Kneib, A. de Mattia, W. J. Percival, G. Rossi, R. Tojeiro *et al.*, Mon. Not. R. Astron. Soc. **500**, 736 (2021).

[6] J. Hou, A. G. Sánchez, A. J. Ross, A. Smith, R. Neveux, J. Bautista, E. Burtin, C. Zhao, R. Scoccimarro, K. S. Dawson, A. de Mattia, A. de la Macorra, H. du Mas des Bourboux, D. J. Eisenstein, H. Gil-Marín *et al.*, Mon. Not. R. Astron. Soc. **500**, 1201 (2021).
[7] R. Neveux, E. Burtin, A. de Mattia, A. Smith, A. J. Ross, J. Hou, J. Bautista, J. Brinkmann, C.-H. Chuang, K. S. Dawson, H. Gil-Marín, B. W. Lyke, A. de la Macorra, H. du Mas des Bourboux, F. G. Mohammad *et al.*, Mon. Not. R. Astron. Soc. **499**, 210 (2020).
[8] S. Alam, M. Aubert, S. Avila, C. Balland, J. E. Bautista, M. A. Bershady, D. Bizyaev, M. R. Blanton, A. S. Bolton, J. Bovy, J. Brinkmann, J. R. Brownstein, E. Burtin, S. Chabanier, M. J. Chapman *et al.*, Phys. Rev. D **103**, 083533 (2021).
[9] T. M. C. Abbott, M. Aguena, A. Alarcon, S. Allam, O. Alves, A. Amon, F. Andrade-Oliveira, J. Annis, S. Avila, D. Bacon, E. Baxter, K. Bechtol, M. R. Becker, G. M. Bernstein, S. Bhargava *et al.*, Phys. Rev. D **105**, 023520 (2022).
[10] T. M. C. Abbott, M. Aguena, S. Allam, A. Amon, F. Andrade-Oliveira, J. Asorey, S. Avila, G. M. Bernstein, E. Bertin, A. Brandao-Souza, D. Brooks, D. L. Burke, J. Calcino, H. Camacho, A. Carnero Rosell *et al.*, Phys. Rev. D **105**, 043512 (2022).
[11] S. Nadathur, W. J. Percival, F. Beutler, and H. A. Winther, Phys. Rev. Lett. **124**, 221301 (2020).
[12] S. Brieden, H. Gil-Marín, and L. Verde, J. Cosmol. Astropart. Phys. 08 (2022) 024.
[13] D. J. Eisenstein, I. Zehavi, D. W. Hogg, R. Scoccimarro, M. R. Blanton, R. C. Nichol, R. Scranton, H.-J. Seo, M. Tegmark, Z. Zheng, S. F. Anderson, J. Annis, N. Bahcall, J. Brinkmann, S. Burles *et al.*, Astrophys. J. **633**, 560 (2005).
[14] S. Cole, W. J. Percival, J. A. Peacock, P. Norberg, C. M. Baugh, C. S. Frenk, I. Baldry, J. Bland-Hawthorn, T. Bridges, R. Cannon, M. Colless, C. Collins, W. Couch, N. J. G. Cross, G. Dalton *et al.*, Mon. Not. R. Astron. Soc. **362**, 505 (2005).
[15] S. Satpathy, S. Alam, S. Ho, M. White, N. A. Bahcall, F. Beutler, J. R. Brownstein, C.-H. Chuang, D. J. Eisenstein, J. N. Grieb, F. Kitaura, M. D. Olmstead, W. J. Percival, S. Salazar-Albornoz, A. G. Sánchez *et al.*, Mon. Not. R. Astron. Soc. **469**, 1369 (2017).
[16] F. Beutler, H.-J. Seo, S. Saito, C.-H. Chuang, A. J. Cuesta, D. J. Eisenstein, H. Gil-Marín, J. N. Grieb, N. Hand, F.-S. Kitaura, C. Modi, R. C. Nichol, M. D. Olmstead, W. J. Percival, F. Prada *et al.*, Mon. Not. R. Astron. Soc. **466**, 2242 (2017).
[17] C. Alcock and B. Paczynski, Nature (London) **281**, 358 (1979).
[18] S. Nadathur, P. M. Carter, W. J. Percival, H. A. Winther, and J. E. Bautista, Phys. Rev. D **100**, 023504 (2019).
[19] H. du Mas des Bourboux, J. Rich, A. Font-Ribera, V. de Sainte Agathe, J. Farr, T. Etourneau, J.-M. Le Goff, A. Cuceu, C. Balland, J. E. Bautista, M. Blomqvist, J. Brinkmann, J. R. Brownstein, S. Chabanier, E. Chaussidon *et al.*, Astrophys. J. **901**, 153 (2020).
[20] R. Ahumada, C. A. Prieto, A. Almeida, F. Anders, S. F. Anderson, B. H. Andrews, B. Anguiano, R. Arcodia, E. Armengaud, M. Aubert, S. Avila, V. Avila-Reese, C. Badenes, C. Balland, K. Barger *et al.*, Astrophys. J. Suppl. Ser. **249**, 3 (2020).
[21] D. J. Eisenstein, D. H. Weinberg, E. Agol, H. Aihara, C. Allende Prieto, S. F. Anderson, J. A. Arns, É. Aubourg, S. Bailey, E. Balbinot, R. Barkhouser, T. C. Beers, A. A. Berlind, S. J. Bickerton, D. Bizyaev *et al.*, Astron. J. **142**, 72 (2011).
[22] K. S. Dawson, J.-P. Kneib, W. J. Percival, S. Alam, F. D. Albareti, S. F. Anderson, E. Armengaud, É. Aubourg, S. Bailey, J. E. Bautista, A. A. Berlind, M. A. Bershady, F. Beutler, D. Bizyaev, M. R. Blanton *et al.*, Astron. J. **151**, 44 (2016).
[23] B. W. Lyke, A. N. Higley, J. N. McLane, D. P. Schurhammer, A. D. Myers, A. J. Ross, K. Dawson, S. Chabanier, P. Martini, N. G. Busca, H. d. Mas des Bourboux, M. Salvato, A. Streblyanska, P. Zarrouk, E. Burtin *et al.*, Astrophys. J. Suppl. Ser. **250**, 8 (2020).
[24] A. Lewis, A. Challinor, and A. Lasenby, Astrophys. J. **538**, 473 (2000).
[25] D. Kirkby, D. Margala, A. Slosar, S. Bailey, N. G. Busca, T. Delubac, J. Rich, J. E. Bautista, M. Blomqvist, J. R. Brownstein, B. Carithers, R. A. C. Croft, K. S. Dawson, A. Font-Ribera, J. Miralda-Escudé *et al.*, J. Cosmol. Astropart. Phys. 03 (2013) 024.
[26] A. Cuceu, A. Font-Ribera, P. Martini, B. Joachimi, S. Nadathur, J. Rich, A. X. González-Morales, H. du Mas des Bourboux, and J. Farr, arXiv:2209.12931.
[27] https://github.com/andreicuceu/vega.
[28] See Supplemental Material at http://link.aps.org/supplemental/10.1103/PhysRevLett.130.191003 for a detailed description of the data, model, and the various robustness tests we performed.
[29] K. M. Górski, E. Hivon, A. J. Banday, B. D. Wandelt, F. K. Hansen, M. Reinecke, and M. Bartelmann, Astrophys. J. **622**, 759 (2005).
[30] J. E. Bautista, N. G. Busca, J. Guy, J. Rich, M. Blomqvist, H. du Mas des Bourboux, M. M. Pieri, A. Font-Ribera, S. Bailey, T. Delubac, D. Kirkby, J.-M. Le Goff, D. Margala, A. Slosar, J. A. Vazquez *et al.*, Astron. Astrophys. **603**, A12 (2017).
[31] H. du Mas des Bourboux, J.-M. Le Goff, M. Blomqvist, N. G. Busca, J. Guy, J. Rich, C. Yèche, J. E. Bautista, É. Burtin, K. S. Dawson, D. J. Eisenstein, A. Font-Ribera, D. Kirkby, J. Miralda-Escudé, P. Noterdaeme *et al.*, Astron. Astrophys. **608**, A130 (2017).
[32] H. du Mas des Bourboux, J. Rich, A. Font-Ribera, V. de Sainte Agathe, J. Farr, T. Etourneau, J.-M. Le Goff, A. Cuceu, C. Balland, J. E. Bautista, M. Blomqvist, J. Brinkmann, J. R. Brownstein, S. Chabanier, E. Chaussidon *et al.*, picca: Package for Igm Cosmological-Correlations Analyses, Astrophysics Source Code Library, record ascl:2106.018 (2021), ascl:2106.018.
[33] C. Ramírez-Pérez, J. Sanchez, D. Alonso, and A. Font-Ribera, J. Cosmol. Astropart. Phys. 05 (2022) 002.
[34] J. Farr, A. Font-Ribera, H. du Mas des Bourboux, A. Muñoz-Gutiérrez, F. J. Sánchez, A. Pontzen, A. Xochitl González-Morales, D. Alonso, D. Brooks, P. Doel, T. Etourneau, J. Guy, J.-M. Le Goff, A. de la Macorra, N. Palanque-Delabrouille *et al.*, J. Cosmol. Astropart. Phys. 03 (2020) 068.

[35] V. de Sainte Agathe, C. Balland, H. du Mas des Bourboux, N. G. Busca, M. Blomqvist, J. Guy, J. Rich, A. Font-Ribera, M. M. Pieri, J. E. Bautista, K. Dawson, J.-M. Le Goff, A. de la Macorra, N. Palanque-Delabrouille, W. J. Percival *et al.*, Astron. Astrophys. **629**, A85 (2019).
[36] A. Arinyo-i-Prats, J. Miralda-Escudé, M. Viel, and R. Cen, J. Cosmol. Astropart. Phys. 12 (2015) 017.
[37] J. J. Givans, A. Font-Ribera, A. Slosar, L. Seeyave, C. Pedersen, K. K. Rogers, D. Blas, and V. Iršič, J. Cosmol. Astropart. Phys. 09 (2022) 070.
[38] W. J. Percival and M. White, Mon. Not. R. Astron. Soc. **393**, 297 (2009).
[39] A. Cuceu, A. Font-Ribera, B. Joachimi, and S. Nadathur, Mon. Not. R. Astron. Soc. **506**, 5439 (2021).
[40] S. Gontcho A Gontcho, J. Miralda-Escudé, and N. G. Busca, Mon. Not. R. Astron. Soc. **442**, 187 (2014).
[41] K. K. Rogers, S. Bird, H. V. Peiris, A. Pontzen, A. Font-Ribera, and B. Leistedt, Mon. Not. R. Astron. Soc. **476**, 3716 (2018).
[42] A. Font-Ribera, E. Arnau, J. Miralda-Escudé, E. Rollinde, J. Brinkmann, J. R. Brownstein, K.-G. Lee, A. D. Myers, N. Palanque-Delabrouille, I. Pâris, P. Petitjean, J. Rich, N. P. Ross, D. P. Schneider, and M. White, J. Cosmol. Astropart. Phys. 05 (2013) 018.
[43] S. Youles, J. E. Bautista, A. Font-Ribera, D. Bacon, J. Rich, D. Brooks, T. M. Davis, K. Dawson, G. Dhungana, P. Doel, K. Fanning, E. Gaztañaga, S. G. A. Gontcho, A. X. Gonzalez-Morales, J. Guy *et al.*, Mon. Not. R. Astron. Soc. **516**, 421 (2022).
[44] B. Abareshi, J. Aguilar, S. Ahlen, S. Alam, D. M. Alexander, R. Alfarsy, L. Allen, C. Allende Prieto, O. Alves, J. Ameel, E. Armengaud, J. Asorey, A. Aviles, S. Bailey, A. Balaguera-Antolínez *et al.*, Astron. J. **164**, 207 (2022).
[45] J. Torrado and A. Lewis, Cobaya: Bayesian analysis in cosmology, Astrophysics Source Code Library, record ascl:1910.019 (2019), ascl:1910.019.
[46] J. Torrado and A. Lewis, J. Cosmol. Astropart. Phys. 05 (2021) 057.
[47] W. J. Handley, M. P. Hobson, and A. N. Lasenby, Mon. Not. R. Astron. Soc. **450**, L61 (2015).
[48] W. J. Handley, M. P. Hobson, and A. N. Lasenby, Mon. Not. R. Astron. Soc. **453**, 4384 (2015).
[49] Note that the choice of isotropic scale parameter is an arbitrary one and not based on arguments about the optimal parameter to measure.
[50] Tension metrics were computed from the full posterior distributions by summing over probability densities.
[51] https://pla.esac.esa.int//##cosmology.
[52] É. Aubourg, S. Bailey, J. E. Bautista, F. Beutler, V. Bhardwaj, D. Bizyaev, M. Blanton, M. Blomqvist, A. S. Bolton, J. Bovy, H. Brewington, J. Brinkmann, J. R. Brownstein, A. Burden, N. G. Busca *et al.*, Phys. Rev. D **92**, 123516 (2015).
[53] R. J. Cooke, M. Pettini, and C. C. Steidel, Astrophys. J. **855**, 102 (2018).
[54] V. Mossa, K. Stöckel, F. Cavanna, F. Ferraro, M. Aliotta, F. Barile, D. Bemmerer, A. Best, A. Boeltzig, C. Broggini, C. G. Bruno, A. Caciolli, T. Chillery, G. F. Ciani, P. Corvisiero *et al.*, Nature (London) **587**, 210 (2020).
[55] F. Gerardi, A. Cuceu, A. Font-Ribera, B. Joachimi, and P. Lemos, Mon. Not. R. Astron. Soc. **518**, 2567 (2022).
[56] A. Lewis, arXiv:1910.13970.
[57] C. R. Harris, K. J. Millman, S. J. van der Walt, R. Gommers, P. Virtanen, D. Cournapeau, E. Wieser, J. Taylor, S. Berg, N. J. Smith, R. Kern, M. Picus, S. Hoyer, M. H. van Kerkwijk, M. Brett *et al.*, Nature (London) **585**, 357 (2020).